Electronic Supplementary Material (ESI) for Nanoscale.

Supplementary Information

Lithographic in-mold patterning for $CsPbBr_3$ nanocrystals distributed Bragg reflector single-mode laser

A. Syazwan A. Kamal,[a] Cheng-Chieh Lin,[b,c,d] Di Xing,[a] Yang-Chun Lee,[a] Zhiyu Wang,[a] Mu-Hsin Chen,[a] Ya-Lun Ho*[a], Chun-Wei Chen[b,c,e] and Jean-Jacques Delaunay*[a]

[a.] *School of Engineering, The University of Tokyo, 7-3-1 Hongo, Bunkyo-ku, Tokyo 113-8656, Japan. E-mail: ho.ya-lun@scale.t.u-tokyo.ac.jp, jean@mech.t.u-tokyo.ac.jp*

[b.] *International Graduate Program of Molecular Science and Technology (NTU-MST), Taiwan International Graduate Program, National Taiwan University and Academia Sinica, Taipei 10617, Taiwan*

[c.] *Department of Materials Science and Engineering, National Taiwan University, Taipei 10617, Taiwan.*

[d.] *Molecular Science and Technology Program, Taiwan International Graduate Program (TIGP), Academia Sinica, Taipei 11529, Taiwan*

[e.] *Center of Atomic Initiative for New Materials (AI-MAT), National Taiwan University, Taipei 10617, Taiwan*

Experimental Section

Chemicals and Reagents. Lead (II) bromide ($PbBr_2$, 99%) was purchased from Sigma-Aldrich. Oleylamine (OLA, 95 %), 1-octadecene (ODE, technical grade 90%), n-hexane (Hex, extra dry, with a molecular sieve, water < 50 ppm), ethyl acetate (EA, 99.5%), and methyl ethyl ketone (MEK, 99%) were purchased from ACROS. Oleic acid (OA, laboratory reagent grade 70%) was purchased from Fisher Scientific. Cesium carbonate (Cs_2CO_3, ReagentPlus®, 99%) was purchased from Sigma-Aldrich. All chemicals were used as received without further purification.

Synthesis of $CsPbBr_3$ Nanocrystals. The synthesis of the perovskite nanocrystals was based on the method introduced by Yakunin et al.[1] The first step is to prepare the Cs-oleate precursor. 0.4 g of Cs_2CO_3, 1.2 mL oleic acid, and 15 mL 1-octadecene was heated in a three-necked flask at 120 ℃ for 1 hour inside a vacuum environment. After that, the temperature increased to 150 ℃ for 25 minutes. The next step is to mix 0.069 g $PbBr_2$ powder with 5 mL of 1-octadecene inside a 25 mL three-necked flask. The solution was then heated to 120 ℃ for 1 hour inside a vacuum environment. Then, the temperature was increased to 130 ℃ inside an argon environment. At the same time, 0.5 mL of oleic acid and 0.5 mL of oleylamine were added to the mixture. After the $PbBr_2$ powder dissolved completely, the mixture was added with 0.4 mL of the Cs-oleate precursor, and it was cooled immediately to room temperature. This step produced the $CsPbBr_3$ perovskite in the form of a precipitate. After that, ethyl acetate (EA) and methyl ethyl ketone (MEK) solvent mixture (EA:MEK = 1:9) was used twice to isolate and purify the synthesized $CsPbBr_3$ nanocrystals. For the final step, the nanocrystals were dispersed in n-hexane and centrifuged at 4000 rpm.

Numerical Simulation. The electric field distributions of the modes and light propagation behavior were computed by using COMSOL (COMSOL Multiphysics, COMSOL, Inc.,

Burlington, U.S.A.), which is a finite element analysis software. The refractive index of ZEP520A was set to 1.55,[2] and the refractive index of $CsPbBr_3$ was set to 1.9.[3] Other materials were modeled using literature values.[4,5] In the frequency domain analysis, the model was surrounded by a perfectly matched layer to absorb scattered light.

Optical Measurements. The schematic illustration of the setup used in the characterization of the lasing performance is shown in Figure S1. An optical parametric amplifier (Orpheus-HP, Light Conversion, Vilnius, Lithuania) with an output wavelength of 400 nm and a 250 fs pulse with a 75 kHz repetition rate was used as the pump light of the fabricated laser structures. A dichroic mirror was used to separate the pump light (λ = 400 nm) from the emitted light (λ > 420 nm). An objective lens with a magnification of ×50 and a numerical aperture of 0.5 was used to focus the pump light onto the fabricated laser structures. Because the calculation of the pump energy density of the lasing threshold depends on the spot size of the pump light, the spot size after the objective lens was estimated by fitting a Gaussian beam distribution to the color levels of the CMOS camera, as shown in the inset of Figure S1. The diameter of the focused pump light spot was estimated to be 50 μm. The emitted light was coupled into an optical fiber using an objective lens with a magnification of ×10 and then the optical fiber was used to inject light into a spectrometer (IsoPlane 160, Princeton Instruments, Trenton, USA) with an optical fiber. For the polarization study, a polarizer was placed in front of the ×10 objective lens.

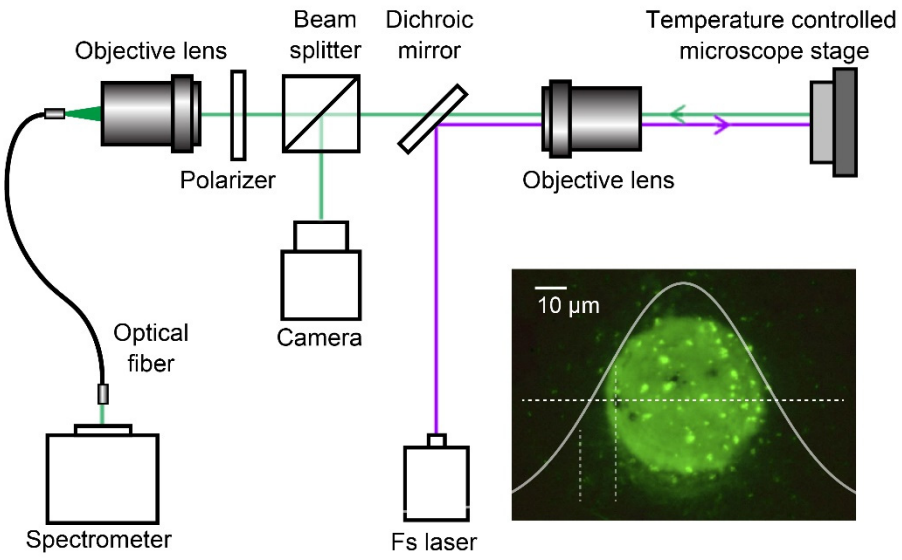

Figure S1. The schematic illustration of the setup for optical measurements.

Table S1. Characteristics of the patterning methods for perovskite nanolasers.

Material	Method	Shape	Lasing type	Single -mode	FWHM (nm)	Year	Ref
$MAPbBr_3$	Lithography + Etching	Disc	WGM[a]	×	0.08	2017	[6]
$MAPbX_3$	Template-confined solution growth	Wire	F-P[b]	×	0.6	2017	[7]
$(BA)_2(MA)_{n-1}Pb_nBr_{3n+1}$	Template-confined solution growth	Ring	WGM	×	0.21	2017	[8]
$MAPbI_3$	Lithography + Spin-coating	Ring	WGM	×	NA	2017	[9]
$MAPbX_3$	Lithography + Etching	Disc	WGM	×	0.4	2018	[10]
$MAPbI_3$	Lithography + Etching	Disc	WGM	○	1.1	2018	[11]
$CsPbX_3$	Lithography + Lift-off	Disc	WGM	×	0.8	2018	[12]
$MAPbBr_xI_y$	Femtosecond laser direct writing	Disc	WGM	○	0.14	2019	[13]
$CsPbBr_3$	Template-confined solution growth	Wire	F-P	○	0.35	2019	[14]
$FAPbI_3$	Femtosecond laser direct writing	Disc	WGM	×	1.88	2020	[15]
$MAPbI_3$	Femtosecond laser direct writing	Wire	F-P	○	0.26	2020	[16]
$FAPbI_3$	Femtosecond laser direct writing	Polygon	WGM	×	0.62	2021	[17]
$CsPbBr_3$	Lithography + Lift-off	Ring/ Disc	WGM	○	0.24	2021	[18]
$CsPbBr_3$	Lithographic in-mold pattering	DBR[c]	F-P	○	0.4	This work	

[a]WGM: whispering gallery mode

[b]F-P: Fabry-Perot

[c]DBR: distributed Bragg reflector

Gratings Design and Optimization

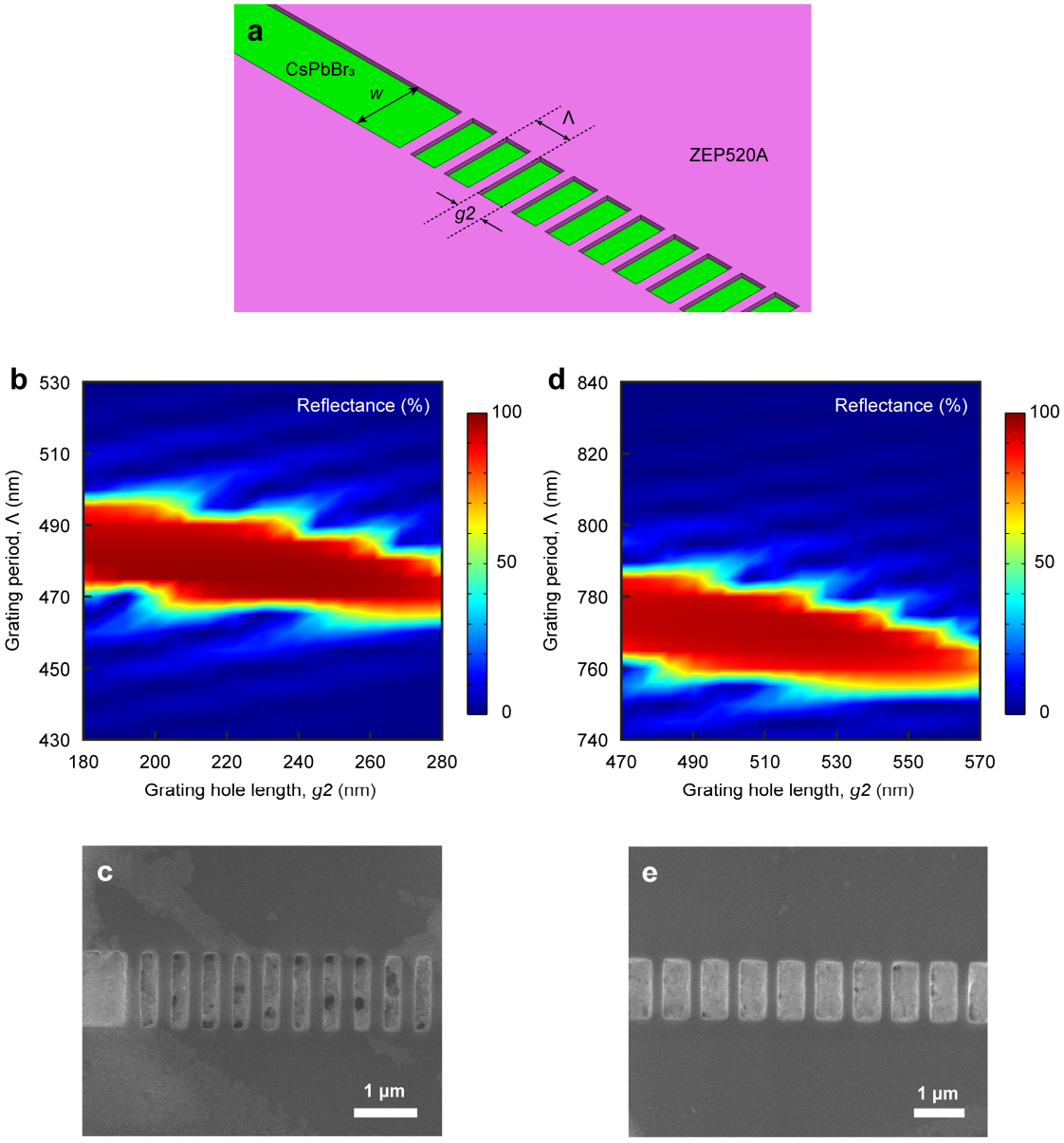

Figure S2. Grating parameters optimization process. (a) The schematic of the grating structure with the definition of the grating period, Λ, the width of the waveguide section and grating holes, *w*, and the length of grating holes, *g*2. (b) The simulated reflectance (%) plot for the third-order Bragg grating. (c) The SEM image of the fabricated third-order Bragg grating, where the measured grating parameters are Λ = 490 nm and *g*2 = 260 nm. (d) The simulated reflectance (%) plot for the fifth-order Bragg grating. (e) The SEM image of the fabricated fifth-order Bragg grating, where the measured grating parameters are Λ = 780 nm and *g*2 = 540 nm.

In the following, the determination of the DBR parameters is explained. The first step is to estimate the grating period by using the first-order Bragg condition $\Lambda = \lambda/(2n_{\text{eff}})$,[19] where Λ is the grating period, λ the wavelength in vacuum, and n_{eff} the effective mode index. In this estimation, λ was set to be 530 nm, and n_{eff} was set to be 1.83, which is obtained from the optical mode analysis, as implemented in COMSOL, performed on the cross-section of the waveguide section perpendicular to the waveguide axis. From these values, the grating period is calculated to be 145 nm. Since the first-order Bragg grating is relatively difficult to fabricate due to the small structure size, a higher-order Bragg grating is considered for the fabrication. In this view, we first chose the third-order Bragg grating, where the Λ was estimated to be 435 nm. To get a more accurate estimation of the grating parameters, a parametric sweep frequency domain analysis was performed using COMSOL, where Λ was varied from 430 to 530 nm, and the grating holes length, *g2*, was varied from 180 to 280 nm. The definition of Λ, *g2*, and *w* are given in Figure S2a. The result of the simulation is shown in Figure S2b, where the reflectance (%) of the grating was plotted with respect to Λ and *g2*. The result shows that the best parameters are Λ = 475 nm and *g2* = 225 nm, where the reflectance is 97.9%. With these parameters as the reference, we fabricated the laser and the SEM image of the laser grating is shown in Figure S2c, where the measured grating parameters are Λ = 490 nm and *g2* = 260 nm. From the figure, it can be observed that there are a lot of defects or pores inside the perovskite region of the grating. These defects will reduce the reflectivity of the grating, which then causes the laser to not be able to lase at room temperature. Because of this, we selected the fifth-order Bragg grating, where the Λ was estimated to be 790 nm. The same simulation as before was performed, where Λ was varied from 740 to 840 nm, and g2 was varied from 470 to 570 nm. The result of the simulation is shown in Figure S2d, where the reflectance (%) of the grating was plotted with respect to Λ and *g2*. The result shows that the best parameters are Λ = 770 nm and *g2* = 520 nm, where the reflectance is 95.2%.

With these parameters as the reference, we fabricated the laser structure and show an SEM image of the laser grating in Figure S2e. The measured grating parameters are Λ = 780 nm and *g2* = 540 nm. Figure S2e reveals a laser structure with no large defects in the perovskite region so that this fabricated laser structure ensures that the grating provides better optical feedback. Indeed, it was found that this laser structure is capable of lasing at room temperature. To further analyze the fabricated fifth-order Bragg grating, a parametric sweep frequency domain analysis was performed using COMSOL, where λ was varied from 525 nm to 535 nm. It was found out that the reflectance of the grating is 70% when λ = 532 nm, and 91% when λ = 533 nm.

$CsPbBr_3$ Perovskite Nanocrystals Stability Study

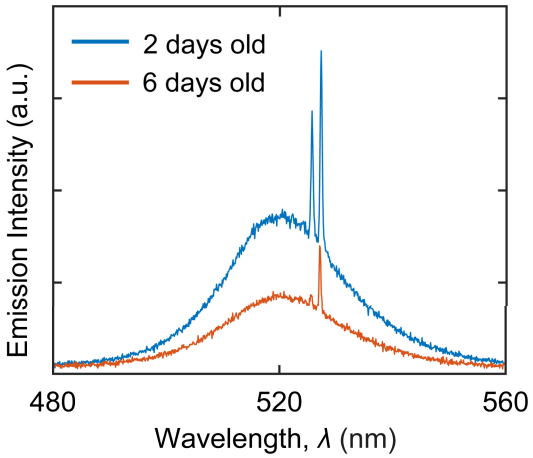

Figure S3. Stability study of the $CsPbBr_3$ perovskite nanocrystals. The blue curve is the output spectrum of the laser when it is 2-day old, and the orange curve is the output spectrum when the laser is 6-day old.

To study the stability of the perovskite nanocrystals, a fabricated laser was analyzed twice with a gap of 4 days in between those tests. The laser was fabricated on June 30, 2020, and was stored in a low vacuum (20 kPa) chamber. After two days in the vacuum chamber, the laser was analyzed by using the optical measurement setup in an ambient atmosphere with a relative humidity of 64%. The sample was exposed to this atmosphere for 10 hours. After that, the laser was stored again in the low vacuum chamber for another 4 days. Finally, another measurement was performed on the laser after 6 days from the fabrication date.

The result of this study is shown in Figure S3. The blue curve is the output spectrum of the laser after 2 days from the fabrication, and the orange curve is the output spectrum after 6 days from the fabrication date. For both measurements, the pump energy density used was 27.5 $\mu J/cm^2$. From Figure S3, the lasing peaks and the photoluminescence peak of the 6 days old laser sample are relatively weaker compared to that of those peaks measured 2 days after the fabrication,

which shows that the perovskite nanocrystals slowly deteriorate over time when kept in a low vacuum and/or relatively high humidity environments. However, as the lasing threshold is 23 $\mu J/cm^2$, it can be concluded that the deterioration was not significant since lasing is still observed at 27.5 $\mu J/cm^2$.

Laser Cavity and Waveguide Light Coupling Simulation Result

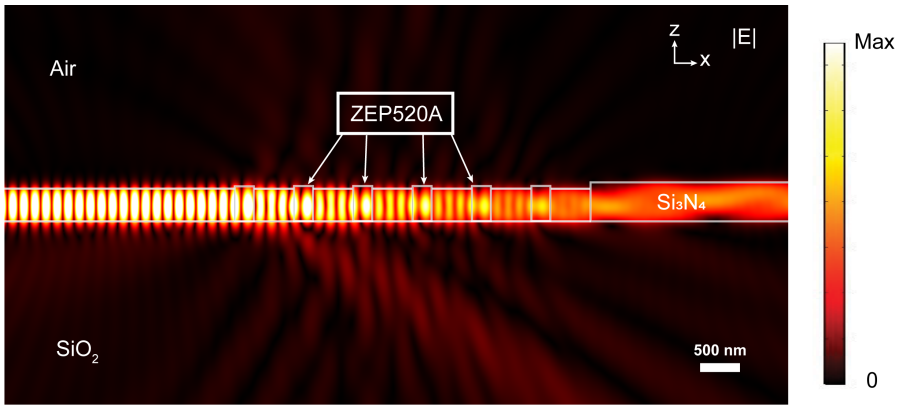

Figure S4. Cross-section along the laser cavity axis showing the simulated electric field norm distribution in a structure consisting of a lasing grating structure and a Si_3N_4 waveguide. The emitted light is coupled to a Si_3N_4 waveguide near the end of the lasing grating structure.

The fabricated lasers are envisioned to be coupled to waveguides to realize photonic integrated circuits. In Figure S4, the electric field distribution in such a structure consisting of a lasing grating structure and a Si_3N_4 waveguide is provided, and it reveals light coupling into the waveguide. A 530 nm light in the form of propagating fundamental waveguide mode was injected into the lasing cavity from the left boundary of the structure. The light then travels through the waveguide section of the laser cavity, reaches the grating structure, is partly reflected into the waveguide section, and is partly transmitted into the Si_3N_4 waveguide at the right side of the simulation domain. The coupling efficiency into the Si_3N_4 waveguide can be controlled by increasing or reducing the number of the grating holes.

The Effect of the Cavity Length on the Laser's Lasing Threshold and Q-factor

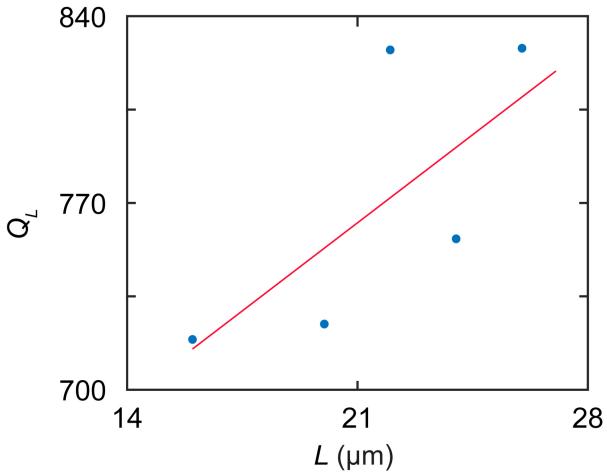

Figure S5. Scatter diagram showing the lasers Q-factor Q_L versus the length L of the waveguide section of the lasers.

The effect of the waveguide section length on the lasing threshold can be evaluated theoretically by using the equation $g_{threshold} = \alpha_0 - (1/2L)\times\ln(R_1\times R_2)$, where $g_{\text{threshold}}$ is the gain threshold, α_0 is the propagation loss inside the waveguide, L is the cavity length of the laser, and R_1 and R_2 are the reflection coefficients of the DBR at each end of the laser.[20] By assuming α_0, R_1, and R_2 to be the same for all lasers, it can be seen from the above equation that by shortening the cavity length, the gain threshold will increase. This also means that by shortening the cavity length, the required pump energy density for the lasing will increase. Our lasing structures should follow this behavior.

In the following, the observed Q-factors of the laser cavities are used to discuss losses. For a laser, its Q-factor while it is lasing can be defined as the ratio of the lasing light energy that is trapped inside the cavity to the energy loss per oscillation cycle.[19,20] This also means that the

higher the Q-factor of the laser is, the lower the lasing threshold will be, due to the low loss in the cavity.[21] From this definition, we can analyze the effect of the laser cavity length on the lasing threshold. The Q-factor of the laser Q_L can be calculated from the laser's output spectrum using the equation $Q_L = f_L/\Delta f$, where f_L is the lasing frequency and Δf is the FWHM of the laser output spectrum in the frequency domain.[19,20] The result of the calculation of the Q-factor for laser cavities with different lengths is plotted in Figure S5. It is noted that all lasers used in this analysis were fabricated on the same chip with the same batch of $CsPbBr_3$ perovskite nanocrystals. This condition is important to ensure that the quality of the fabrication and the amount of gain provided by the perovskite material can be assumed to be the same for all lasers. Figure S5 shows that the Q-factor increases with the cavity length. This trend confirms that the cavity becomes lossier when the cavity length becomes shorter, and so the lasing threshold increases when the cavity length decreases.

References

1. S. Yakunin, L. Protesescu, F. Krieg, M. I. Bodnarchuk, G. Nedelcu, M. Humer, G. De Luca, M. Fiebig, W. Heiss, M. V. Kovalenko, *Nat. Commun.*, 2015, **6**, 8056.

2. Zeon Corporation, 2003, ZEP520A: Technical Report. Tokyo, Japan.

3. W. Yan, L. Mao, P. Zhao, A. Mertens, S. Dottermusch, H. Hu, Z. Jin, and B. S. Richards, *Opt. Express*, 2020, **28**, 15706.

4. P. E. Ciddor, *Appl. Opt.*, 1996, **35**, 1566.

5. I. H. Malitson, *J. Opt. Soc. Am*., 1965, **55**, 1205.

6. N. Zhang, W. Sun, S. P. Rodrigues, K.Wang, Z. Gu, S. Wang, W. Cai, S. Xiao and Q. Song, *Adv. Mater.*, 2017, **29**, 1606205.

7. P. Liu, X. He, J. Ren, Q. Liao, J. Yao and H. Fu, *ACS Nano*, 2017, **11**, 5766.

8. H. Zhang, Q. Liao, Y. Wu, Z. Zhang, Q. Gao, P. Liu, M. Li, J. Yao and H. Fu, *Adv. Mater.*, 2018, **30**, 1706186.

9. P. J. Cegielski, S. Neutzner, C. Porschatis, H. Lerch, J. Bolten, S. Suchow, A. R. S. Kandada, B. Chmielak, A. Petrozza, T. Wahlbrink, and A. L. Giesecke, *Opt. Express*, 2017, **25**, 13199.

10. S. Wang, Y. Liu, G. Li, J. Zhang, N. Zhang, S. Xiao and Q. Song, *Adv. Opt. Mater.*, 2018, **6,** 1701266.

11. P. J. Cegielski, A. L. Giesecke, S. Neutzner, C. Porschatis, M. Gandini, D. Schall, C. A. R. Perini, J. Bolten, S. Suckow, S. Kataria, B. Chmielak, T. Wahlbrink, A. Petrozza and M. C. Lemme, *Nano Lett.*, 2018, **18**, 6915.

12. C. H. Lin, Q. Zeng, E. Lafalce, S. Yu, M. J. Smith, Y. J. Yoon, Y. Chang, Y. Jiang, Z. Lin, Z. V. Vardeny and V. V. Tsukruk, *Adv. Opt. Mater.*, 2018, **6**, 1800474.

13. A. Zhizhchenko, S. Syubaev, A. Berestennikov, A. V. Yulin, A. Porfirev, A. Pushkarev, I. Shishkin, K. Golokhvast, A. A. Bogdanov, A. A. Zakhidov, A. A. Kuchmizhak, Y. S. Kivshar and S. V. Makarov, *ACS Nano*, 2019, **13**, 4140.

14. Z. Yang, J. Lu, M. ZhuGe, Y. Cheng, J. Hu, F. Li, S. Qiao, Y. Zhang, G. Hu, Q. Yang, D. Peng, K. Liu and C. Pan, *Adv. Mater.*, 2019, **31**, 1900647.

15. X. Tian, Y. Xu, H. Zhao, X. Qin, Y. Nie, W. Li, S. Liu, Q. Lin and Q. Cao, *J. Mater. Chem. C*, 2020, **8**, 7314.

16. A. Y. Zhizhchenko, P. Tonkaev, D. Gets, A. Larin, D. Zuev, S. Starikov, E. V. Pustovalov, A. M. Zakharenko, S. A. Kulinich, S. Juodkazis, A. A. Kuchmizhak and S. V. Makarov, *Small*, 2020, **16**, 2000410.

17. X. Tian, L. Wang, W. Li, Q. Lin and Q. Cao, *ACS Appl. Mater. Interfaces*, 2021, **13**, 16952.

18. D. Xing, C. C. Lin, Y. L. Ho, A. S. A. Kamal, I. T. Wang, C. C. Chen, C. Y. Wen, C. W. Chen and J. J. Delaunay, *Adv. Funct. Mater.*, 2021, **31**, 2006283.

19. J. T. Verdeyen, *Laser Electronics*, Prentice Hall, New Jersey, 1995.

20. A. Yariv, *Quantum Electronics*, Wiley, 1989.

21. J.-W. Lee, H.-H. Yu, C.-H. Yi, C.-M. Kim, *Opt. Lett.*, 2014, **39**, 2676-2679.